

New mid-infrared optical sources based on isotropic semiconductors (zinc selenide and gallium arsenide) using total internal reflection quasi-phase-matching

R. HAÏDAR^{*1}, PH. KUPECEK², E. ROSENCHER¹, R. TRIBOULET³ and PH. LEMASSON³

¹ONERA/DMPH, Chemin de la Huniere, 91761 Palaiseau cedex, France

²ONERA/DMPH and UPMC, 4 Place Jussieu, 75005 Paris, France

³CNRS Bellevue, 1 place Aristide Briand, 92195 Meudon cedex, France

The French aerospace agency is involved in the realization of compact solid-state coherent sources, such as optical parametric oscillators (OPO), using new materials, such as highly non-linearly efficient semiconductors (ZnSe, GaAs or InP). However, since these materials are optically isotropic, they require new phase-matching techniques. We report the quasi-phase matched difference frequency generation in isotropic semiconductors using total internal reflection. We made use of large Fresnel birefringence at reflection between the signal and idler wave outputs of an OPO. Large tunability (between 8 and 13 μm) is demonstrated. Agreement between theoretical expectation and experimental results is excellent.

Keywords: non-linear optics, difference frequency generation, mid-infrared light, quasi-phase matching, isotropic semiconductors, Fresnel birefringence.

1. Introduction

Mid-infrared (MIR) tunable sources are becoming of considerable interest for applications in environmental monitoring [1]. Optical parametric generation is a good candidate for the production of MIR wavelengths from classical near-infrared sources (Nd:YAG, Er:SiO₂). However, apart from exotic materials (ZnGeP₂, AgGaSe₂), most of the usual nonlinear crystals (LiNbO₃, KTP) absorb strongly above 5 μm . On the opposite, semiconductors of the main technological stream (GaAs, InP, ZnSe) are excellent candidates for optical frequency conversion because of:

- high optical 2nd-order nonlinear susceptibility d ,
- excellent transparency over the 1–15 μm range,
- good mechanical properties,
- technological maturity,
- possibility of future integration with the pumping source [2].

However, most of these materials are isotropic so that no birefringence phase-matching scenarios are available [3]. Recently, alternative techniques have been investigated: artificial birefringence in GaAs/AlO_x waveguides [4], and alternate GaAs stack quasi-phase matching [5,6]. In these experiments, no results of tunability in the 8–12 μm range have been obtained for several reasons: absorption of AlO_x, stack thickness resonance etc.

However, as early as in 1962, Armstrong *et al.* [7] suggested that quasi-phase matching could be obtained by total

internal reflection (TIR-QPM) in a plane-parallel plate, when each leg of the zigzag path in the crystal is approximately an odd integer number of coherence lengths and the relative phase shift between the different waves on each bounce is adjusted by Fresnel phase shift at reflection. This technique was successfully demonstrated for second harmonic generation [8,9] in GaAs, ZnSe or ZnS crystals. Its major advantage is that it requires less stringent technological steps for its realisation, compared to diffusion bonding or waveguide design.

We have adapted TIR-QPM to difference frequency generation (DFG) of near infrared light (~ 2 μm) into the mid-infrared (~ 10 μm) with the following advantages. First, since parallel and perpendicular polarization waves display different reflection coefficients (Fresnel relations [10]), a highly differentiating mechanism between the two pumping waves is obtained, which allows large tunability and greatly alleviates the phase matching conditions. This technique is actually very similar in its principle to the birefringent phase matching, and we call it Fresnel phase matching. Secondly, because of the low optical dispersions displayed by these materials in the MIR range, large coherence lengths and thus high conversion efficiencies are obtained [11].

2. Theoretical background

Figure 1 shows a schematic diagram of the Fresnel TIR-QPM configuration. Input and output coupling occur through the slanted end faces of the monolithic sample. As it can be seen from Fig. 1, the thickness t and the TIR-angle

* e-mail: haidar@onera.fr

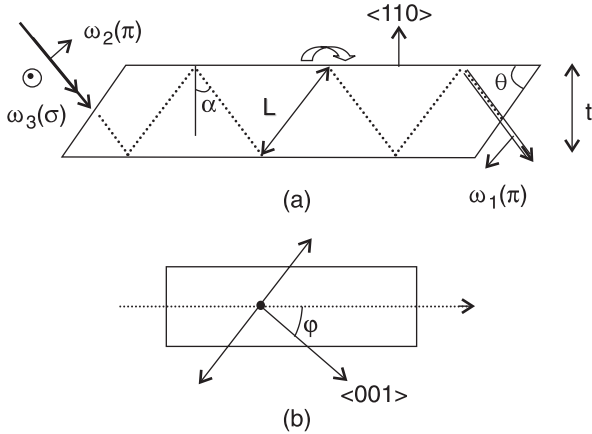


Fig. 1. Schematic diagram of the Fresnel TIR-QPM configuration (a). The angle α is chosen greater than the total internal reflection limit angle. We present here the $\sigma\pi\pi$ polarisation configuration of the three waves. Top-view for angle definition (b).

α are the only geometrical parameters of the plate. They determine the TIR-QPM conditions, i.e., the distance between two TIR bounces and the Fresnel phase shift at reflection.

The pumping beams (circular frequencies ω_2 and ω_3) and the DFG one ($\omega_1 = \omega_3 - \omega_2$) display wavevectors k_i ($i = 1,2,3$) inside the semiconductor. The coherence length of the DFG interaction is $\Lambda_C = \pi/\Delta k$, where $\Delta k = k_3 - k_2 - k_1$ is the wavevector mismatch. In the undepleted pump and plane wave approximations, the output DFG power P_1 is given by [9,12]

$$P_1 = \frac{\chi_{eff}^2}{4c^2} \frac{\omega_1 \omega_2 \omega_3}{n_1 n_2 n_3} L^2 \frac{\sin^2(\Delta k L / 2)}{(\Delta k L / 2)^2} \frac{\sin^2(N \Delta \Phi / 2)}{\sin^2(\Delta \Phi / 2)} P_2 P_3, \quad (1)$$

where P_2 and P_3 are the input wave powers. N is the number of zigzags in the plate. It is a function of the plate's dimensions and of the TIR angle α . $\Delta \Phi$ is the phase error per zigzag path, i.e., $\Delta \Phi = \Delta k L + \Phi_F + \varepsilon \pi$. It is due to the additive contributions of the wavevector mismatch and the Fresnel relative phase shifts of the different waves at reflection ($\Phi_F = \varphi_3 - \varphi_2 - \varphi_1$), ε stands for the eventual change of sign of χ_{eff} at reflection ($\varepsilon = 1$ if change of sign, 0 if not).

One can clearly see from Eq. (1) that, for a given set of pumping waves (i.e., for the given Δk), the DFG mechanism is maximum when, independently, the zigzag path length L is an odd integer number of coherence lengths [$L \approx (2p + 1)\Lambda_C$] and the phase error $\Delta \Phi = 0 \pmod{2\pi}$, so that $\Phi_F(\alpha) + \varepsilon \pi = \pi \pmod{2\pi}$. This latter relation (that we refer to as Fresnel phase matching condition) is an equation determining the TIR angle α which must be higher than the Descartes-Snell angles α_i , $\sin \alpha_i = 1/n(\omega_i)$. Eight different equations are then generated, depending on the different combinations of the polarizations of the three waves ($\omega_3, \omega_2, \omega_1$): $\sigma\sigma\sigma$ and $\pi\pi\pi$ which have no equivalent in birefringence phase matching, $\pi\sigma\sigma$ and $\sigma\pi\pi$ which we can refer to as type I phase matching, and eventually $\pi\pi\sigma$,

$\sigma\pi\sigma$, $\pi\sigma\pi$, and $\sigma\sigma\pi$ which can be referred to as type II phase matching [π (σ) designates an electric field oriented parallel (perpendicular) to the plane of incidence].

2.1. Zinc selenide plates

Careful computation shows that the only practical cases are the type I $\sigma\pi\pi$ and $\pi\sigma\sigma$ polarization configurations (Fig. 2): thanks to a differential Fresnel phase shift of $\Phi_F(\alpha) = 0$ or $\pi \pmod{2\pi}$ for respectively $\alpha \approx 45^\circ$ or 28° (note: the corresponding Descartes-Snell angles are $\alpha_i \leq 25^\circ$ [13]), they both can provide QPM cumulative growth, depending on whether $\varepsilon = 1$ or 0.

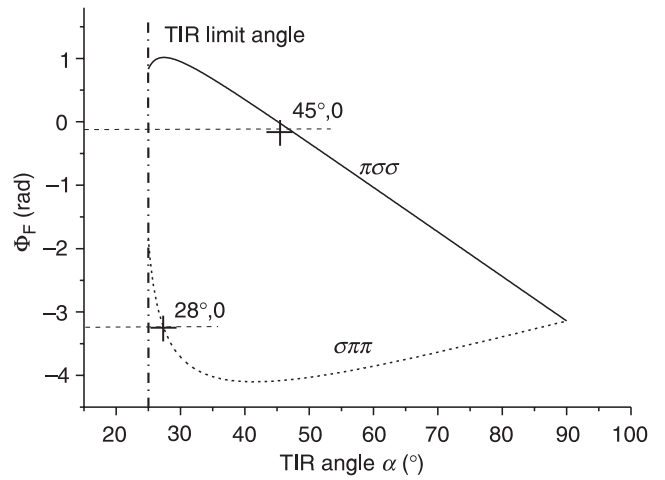


Fig. 2. Relative Fresnel phase shift Φ_F between the 3 waves ($2.38 \mu\text{m} + 1.92 \mu\text{m} \rightarrow 10.0 \mu\text{m}$) at total internal reflection in ZnSe plates as a function of internal angle α . Fresnel phase matching is obtained when $\Phi_F = 0$ or π .

Our ZnSe crystals have been grown by solid-state recrystallisation of high purity polycrystalline plates, the precise description of which can be found in Ref. 14.

2.1.1. The $\sigma\pi\pi$ configuration

Note that small TIR angles α should be preferred for polishing tolerance concerns: indeed, for a given thickness uncertainty δt (typically due to polishing), the knowledge of the interaction length $L = t/\cos \alpha$ and the phase error $\Delta \Phi$ is all the more accurate as α is small. Our first choice is then the $\sigma\pi\pi$ configuration, with a TIR-QPM angle $\alpha \approx 27^\circ$. Practically, we choose the wedge angle θ close to 27° , and by slightly rotating the crystal we can adjust the value of α for TIR-QPM.

Now, if we use $\langle 110 \rangle$ oriented plates [Fig. 1(a)], we get for the $\sigma\pi\pi$ polarization configuration

$$\chi_{eff, \sigma\pi\pi} = \chi^{(2)} \sin \varphi (3(\cos \varphi \cos \alpha)^2 + 1 - 2 \cos^2 \alpha), \quad (2)$$

where φ is the angle between the plane of incidence and the $\langle 001 \rangle$ axis of the ZnSe crystal [Fig. 1(b)]. We then note

that $\chi_{eff,\sigma\pi\pi}(\pi - \alpha) = \chi_{eff,\sigma\pi\pi}(\alpha)$, i.e., there is no sign reversal at reflection, and thus $\Delta\Phi = \Delta kL + \Phi_F$. For $\alpha = 27^\circ$, we eventually expect a maximum value of $\chi_{eff,\sigma\pi\pi} = 94 \text{ pm/V}$ ($\chi^{(2)} = 156 \text{ pm/V}$ [15]) for $\varphi = 30^\circ$.

We can next calculate the optimum thickness t . As the coherence length is almost constant in the 8 to 12 μm range for DFG in ZnSe [11], we choose $\bar{\Lambda}_C \approx 77 \mu\text{m}$ as a mean value: we then adjust the interaction length by slightly tuning the TIR angle α . For experimental convenience, we choose a near-mm thickness: $t \approx 885 \mu\text{m}$, which is a practical dimension and provides an interaction length $L \approx 1002 \mu\text{m} \approx 13 \times \bar{\Lambda}_C$ (13rd order QPM). Our plates are 17 mm long, which provides a geometrical number of TIR bounces $NTIR \approx 29$.

The plates are mechanically polished, which proves to provide mirror-shape surfaces. However, measurements performed with a Talysurf 5–120 profilometer from Taylor-Hobson show that the surfaces are still very rough, with a peak-to-valley value of $p-v \approx 150 \text{ nm}$. We can then estimate the Strehl ratio R which quantifies the impact of the surface quality on the reflectivity [16]

$$R = \exp \left[- \left(\sigma_s \frac{4\pi n}{\lambda_0} \cos \alpha \right)^2 \right], \quad (3)$$

where σ_s is the rugosity standard deviation which, in the Gaussian distribution approximation, is given by

$$\sigma_s \approx \frac{p-v}{12}.$$

This gives a Strehl ratio of $R \approx 97\%$ if $\lambda_0 = 2 \mu\text{m}$ and $\alpha = 27^\circ$, which means that total internal reflection is not as efficient as expected: there is a loss of at least 3% on all the three waves at each TIR bounce. This will introduce high losses in the construction of the DFG wave throughout the plate; and at the same time, it will impose a limit to the number of TIR bounces. We define the effective number of

TIR bounces for a given TIR reflection coefficient $[NTIR_{eff}(R_{TIR})]$ as the number of TIR bounces for a unity reflection coefficient $[NTIR (R = 1)]$ which provides exactly the same DFG yield.

In Fig. 3(a), we represent the effective number of TIR bounces as a function of the TIR reflection coefficient, given that the geometrical number of TIR bounces in our plate is $NTIR \approx 29$. Small variations in the reflection coefficient have drastic effects on the nonlinear conversion yield. As it can be seen in Fig. 3(b), which represents the DFG yield as a function of the geometrical number of TIR bounces for a given reflection coefficient, there also appears to be an optimum, for which the parametric gain is exactly compensated by the reflection losses. This limits the dimensions of the plate, thus the number of useful TIR bounces.

In conclusion, there is a need for a better polishing procedure of our ZnSe plates: many papers [17,18] describe and compare different mechano-chemical polishing procedures for both polycrystalline and monocrystalline ZnSe plates, but with, up to now, very bad results in term of rugosity parameters.

2.1.2. The $\pi\sigma\sigma$ configuration

Thanks to a differential Fresnel phase shift of $\Phi_F(\alpha) = \pi(\text{mod } 2\pi)$ for $\alpha \approx 45^\circ$, we also expect TIR-QPM cumulative growth of the DFG wave in (110) ZnSe providing that the waves are in the $\pi\sigma\sigma$ polarization configuration and that the non-linear coefficient χ_{eff} changes its sign at reflection.

The main advantages of this configuration compared to the one of subsection 2.1.1 are the following:

- with a greater TIR-angle, the rugosity has a lesser influence on the reflection coefficient (Eq. 3),
- since the Descartes-Snell angles are $\alpha_i \leq 25^\circ$, it is more comfortable to work at $\alpha \approx 45^\circ$ than at $\alpha \approx 27^\circ$.

We use <110> oriented plates [Fig. 1(a)], and we get for the $\pi\sigma\sigma$ polarization configuration

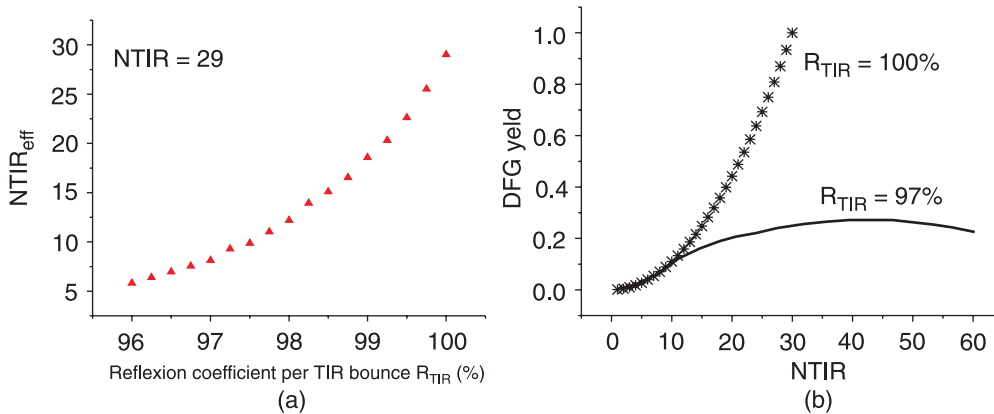


Fig. 3. $NTIR = 29$ in our $\sigma\pi\pi$ -ZnSe plates. We show $NTIR_{eff}$ as a function of the TIR reflection coefficient (a). The Strehl ratio foresees TIR losses of at least 3% per bounce for each wave ($R_{TIR} = 97\%$) (b). This considerably reduces the DFG yield: there is a tight competition between the parametric gain and the cumulative losses what leads to an optimum value of $NTIR$.

$$\chi_{eff,\pi\sigma\sigma} = \frac{1}{4} \chi^{(2)} \cos \alpha (\cos \varphi + 3 \cos(3\varphi)), \quad (4)$$

where φ is the angle between the plane of incidence and the $\langle 001 \rangle$ axis of the ZnSe crystal [Fig. 1(b)]. Then, we note that $\chi_{eff,\pi\sigma\sigma}(\pi - \alpha) = -\chi_{eff,\sigma\pi\pi}(\alpha)$, i.e., there is a sign reversal at reflection, and thus $\Delta\Phi = \Delta kL + \Phi_F + \pi$. For $\alpha = 45^\circ$, we eventually expect a maximum value of $\chi_{eff,\pi\sigma\sigma} = 110 \text{ pm/V}$ ($\chi^{(2)} = 156 \text{ pm/V}$ [15]) for $\varphi = 0^\circ$.

We can next calculate the optimum thickness t . As $\bar{\Lambda}_C \approx 77 \text{ }\mu\text{m}$, we choose a thickness: $t \approx 832 \text{ }\mu\text{m}$, which is a practical dimension and provides an interaction length $L \approx 1176 \text{ }\mu\text{m} \approx 15 \times \bar{\Lambda}_C$ (15th order QPM). Our plates are 16 mm long, which provides a geometrical number of TIR bounces $NTIR \approx 17$.

As in subsection 2.1.1, the plates are mechanically polished; we thus have equivalent surface qualities for both the samples. But, as is said above, the impact of rugosity is compensated for by the higher TIR angle $\alpha = 45^\circ$.

2.2. Gallium arsenide plates

Same considerations as in subsection 2.1 bring the following conclusions: type I TIR quasi phase-matching is possible in GaAs plates (Fig. 4). We choose the $\sigma\pi\pi$ configuration, with a TIR angle $\alpha \approx 20.5^\circ$ (note: the corresponding Descartes-Snell angles are $\alpha_i \leq 18^\circ$ [19]).

As we also use $\langle 110 \rangle$ oriented plates [Fig. 1(a)], we draw the same properties as for $\sigma\pi\pi$ -ZnSe. According to Eq. (2), we note that $\chi_{eff,\sigma\pi\pi}(\pi - \alpha) = \chi_{eff,\sigma\pi\pi}(\alpha)$, i.e., there is no sign reversal at reflection, and thus $\Delta\Phi = \Delta kL + \Phi_F$. And eventually, for $\alpha = 20.5^\circ$, we expect a maximum value of $\chi_{eff,\sigma\pi\pi} = 443 \text{ pm/V}$ ($\chi^{(2)} = 736 \text{ pm/V}$ [15]) for $\varphi = 30^\circ$.

We can next calculate the optimum thickness t . We choose $\bar{\Lambda}_C \approx 33 \text{ }\mu\text{m}$ as a mean value [11] in the 8 to 12 μm range for DFG: we then adjust the interaction length by

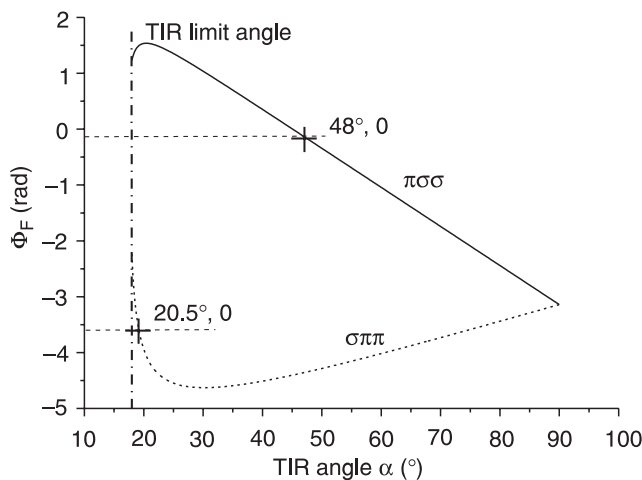


Fig. 4. Relative Fresnel phase shift Φ_F between the 3 waves ($2.38 \text{ }\mu\text{m} + 1.92 \text{ }\mu\text{m} \rightarrow 10.0 \text{ }\mu\text{m}$) at total internal reflection in GaAs plates as a function of internal angle α . Fresnel phase matching is obtained when $\Phi_F = 0$ or π .

slightly tuning the TIR angle α . Our (110) GaAs plates are of a commercial origin (Atomergic Chemetals, Inc.); in order to get the best possible surface quality, we choose them “manufactory” double-faced polished, which actually is a chemico-mechanical polishing and provides excellent rugosity parameters. There is no further polishing of the upper and lower faces. Because of commercial availability, we choose a thickness of $t \approx 400 \text{ }\mu\text{m}$, which provides the interaction length $L \approx 427 \text{ }\mu\text{m} \approx 13 \times \bar{\Lambda}_C$ (13rd order QPM). Our plates are 12 mm long, which provides a geometrical number of TIR bounces $NTIR \approx 65$.

The only mechanical modification is to introduce the slanted faces, with a wedge angle $\theta \approx 20.5^\circ$. We thus dispose of very high quality GaAs plates.

3. Experimental set-up and results

For the DFG experiment, the source is a Nd:YAG pumped LiNbO₃ type I optical parametric oscillator (LN-OPO), with a Littrow-grating for fine tuning [20].

The signal and idler waves, ω_3 and ω_2 , are tunable between 1.8 μm and 2.4 μm (spectral bandwidth around 2 cm^{-1}) with about 10 mJ overall available energy for a pulse duration of 10 ns. As we need crossed polarizations for signal and idler, a LiIO₃ plane parallel phase plate is inserted on the LN-OPO output beam path [20]. DFG energy, which wavelength is deduced from spectrometer-controlled ω_2 and ω_3 , is measured using a photoconducting Graseby HgCdTe detector protected by adequate filtering through reflection-treated germanium plates (Fig. 5). A Judson PA300 preamplifier enhances the electric output of the detector so that we can measure it with an oscilloscope.

For a total incident energy of 150 μJ (idler over signal energy ratio of 10%), we typically get a few hundreds of picojoules of DFG light at 10 μm (Fig. 6). Calibration measurements made on (110) ZnSe prisms (same origin as our

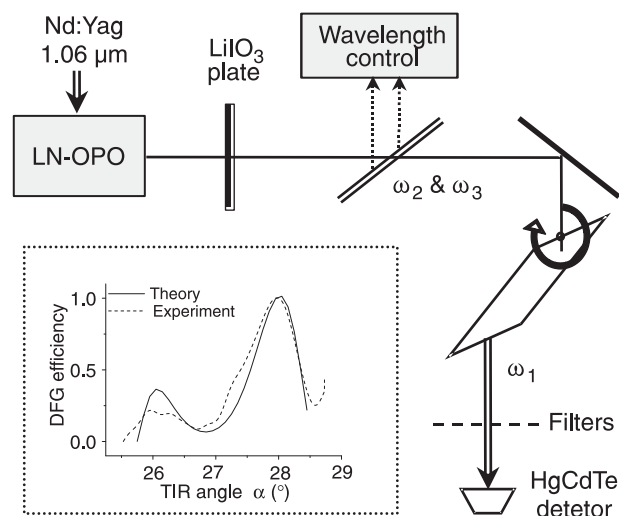


Fig. 5. Experimental set-up for Fresnel TIR-QPM of difference frequency generation in ZnSe and GaAs plates (inset: experimental result and comparison with theory in $\sigma\pi\pi$ -ZnSe).

ZnSe plates [14]) and (111) GaAs prisms [11] (purchased from AXT) indicate that this corresponds to the contribution of respectively 12, 16, and 33 coherence lengths in $\sigma\pi\pi$ -ZnSe, $\pi\sigma\sigma$ -ZnSe and $\sigma\pi\pi$ -GaAs (instead of 29, 17, and 65 geometrically expected). All these results are summarized in Table 1.

Table 1. The experimental details and results for the three tested plates.

	ZnSe	ZnSe	GaAs
Polarization configuration	$\sigma\pi\pi$	$\pi\sigma\sigma$	$\sigma\pi\pi$
Descartes-Snell angle	25°	25°	18°
TIR angle α	25°	45°	20.5°
χ_{eff} (pm/V)	94	110	443
Rugosity $p-v$ (nm)	150	150	Not measured
$NTIR$	29	17	65
$NTIR_{eff}$	12	16	33

As it is shown in Table 1, the $\pi\sigma\sigma$ -ZnSe configuration presents the best $NTIR_{eff}/NTIR$ ratio, despite its poor polishing quality compared to the GaAs plates. An explanation of this may be the following: in the $\pi\sigma\sigma$ -ZnSe configuration, the TIR-QPM angle α is very far from the Descartes-Snell angle, which:

- reduces the influence of rugosity, as has already been said, but this seems not so drastic after all, since the $NTIR_{eff}/NTIR$ ratios are comparable in $\sigma\pi\pi$ -ZnSe and $\sigma\pi\pi$ -GaAs,
- provides a “security margin” for the total reflection process, and thus guarantees a high reflection coefficient at each TIR bounce. The second reason seems eventually to import more than the first one, in terms of nonlinear conversion efficiency.

The inset in Fig. 5 shows both the variations of the normalized DFG detected signal as a function of the TIR angle α , and the normalized theoretical curve obtained through

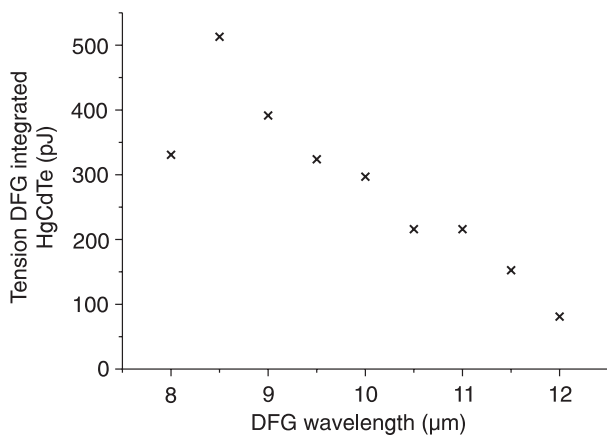


Fig. 6. Spectral emission of the TIR-QPM $\pi\sigma\sigma$ -ZnSe plate. Global incident energy (signal and idler) is 150 μJ.

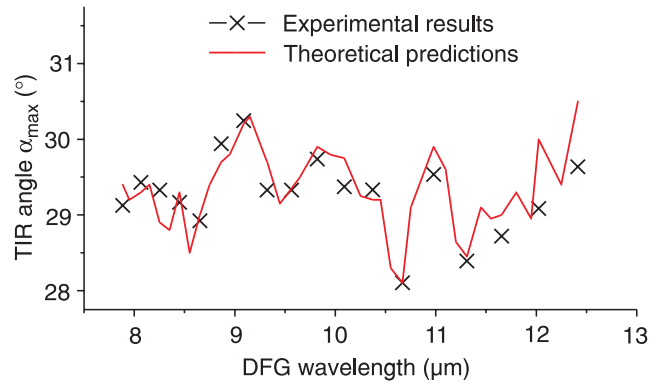


Fig. 7. Fresnel phase matching for DFG in a ZnSe plate; comparison between experiment and theory.

Eq. (1). The agreement between experiment and theory is convincing. Wavelengths ω_3 and ω_2 are then scanned, and TIR-QPM is obtained by slightly rotating the crystal, thus adjusting the value of α .

The phase matching condition is defined when the DFG yield reaches its maximum value, e.g., $\alpha_{max} \approx 28^\circ$ in Fig. 5. The measured values, together with the theoretical computations, are reported in Fig. 7. Since TIR-QPM results from a balance between the interaction length [$L \approx (2p + 1)\Lambda_C$], and the relative phase shift at reflection [$\Delta\Phi = 0 \pmod{2\pi}$], we get a rather complicated curve aspect, which is however correctly predicted by the theory.

Thanks to the high versatility of the TIR-QPM technique applied to a single plate, the emission spectral range is rather large. Figure 6 shows the spectral emission of the $\pi\sigma\sigma$ -ZnSe plate (with TIR-angle α tuned around 45°, so that $NTIR$ is kept constant).

4. Conclusions

In conclusion, we report evidence of quasi-phase matched DFG in ZnSe and GaAs plates using total internal reflection. We made use of the large Fresnel birefringence between the signal and idler wave outputs of an optical parametric oscillator. This provides us with a new compact coherent solid-state MIR (8–12 μm) optical source.

It appears that the main difficulty is to reach high standard of polishing rugosity for the semiconductor plates. As to GaAs, actual polishing methods provide excellent rugosity parameters, which allow being confident in high progress for a close future. Special efforts are still to be made on ZnSe; collaboration with University of Jussieu (Paris, France) on mechano-chemical polishing should lead to results very soon.

Acknowledgement

Part of this work is supported by the European Community within the MOPOSC project (Monolithic OPO using Semiconductor Cavities). The authors would like to thank Y. Lévy, R. Mercier and J. Taboury from the Institut

d'Optique Théorique et Appliquée (Orsay, France) for fruitful discussions.

References

1. See Special issue N° 6, "Laser Applications to chemical and environmental analysis", *Appl. Opt.* **40**, 2001.
2. E. Rosencher, "Towards integrated semiconductor optical parametric oscillators", *CR. Acad. Sci. Paris, Série IV*, 615–625 (2000).
3. E. Rosencher and B. Vinter, *Optoelectronics*, Cambridge University Press, New York, 2002.
4. A. Fiore, V. Berger, E. Rosencher, P. Bravetti, and J. Nagle, "Phase matching using an isotropic nonlinear material", *Nature* **391**, 463–466 (1998).
5. E. Lallier, L. Becouarn, M. Brévignon, and J. Lehoux, "Infrared difference frequency generation with quasi-phase-matched GaAs" *Electron. Lett.* **17**, 212 (1998).
6. L. Gordon, R.C. Eckardt, R.L. Byer, R.K. Route, and R.S. Feigelson, *Ginzton Lab. Rep. 5133*, Ginzton Laboratory, Stanford University, Stanford, Calif, 1992.
7. J. Armstrong, N. Bloembergen, J. Ducuing, and P. Pershan, "Interactions between light waves in a nonlinear dielectric", *Phys. Rev.* **127**, 1918–1939 (1962).
8. G.D. Boyd and C.K.N. Patel, "Enhancement of optical second-harmonic generation by reflection phase matching in ZnS and gas", *Appl. Phys. Lett.* **8**, 313–315 (1966).
9. H. Komine, W.H. Long, J.W. Tully, and E.A. Stappaerts, "Quasi-phase-matched second-harmonic generation by use of a total-internal-reflection phase shift in gallium arsenide and zinc selenide plates", *Optics Lett.* **23**, 661–663 (1998).
10. M.V. Klein and T.E. Furtak, *Optics* (2nd edition), John Wiley, New York, 1998.
11. R. Haidar, A. Mustelier, Ph. Kupecek, E. Rosencher, P. Lemasson, R. Triboulet, and G. Mennerat, "Largely tunable mid-infrared (8–12 μm) difference frequency generation in isotropic semiconductors", *J. Appl. Phys.* **91**, 2550–2553 (2002).
12. N. Forget, *Rapport de stage de l'Ecole Polytechnique*, ONERA, Palaiseau, 2001.
13. H.H. Li, "Refractive index of ZnS, ZnSe, and ZnTe and its wavelength and temperature derivatives", *J. Phys. Chem. Ref. Data* **13**, 103–150 (1984).
14. E. Rzepka, J.P. Roger, P. Lemasson, and R. Triboulet, "Optical transmission of ZnSe crystals grown by solid phase recrystallization", *J. Cryst. Growth* **197**, 480–484 (1999).
15. R. L. Sutherland, *Handbook of Non-linear Optics*, Dekker, New York, 1996.
16. P.K. Tien, "Light waves in thin films and integrated optics", *Appl. Opt.* **10**, 2395–2413 (1971).
17. L.M. Liu, G. Lindauer, W.B. Alexander, and P.H. Holloway, "Surface preparation of ZnSe by chemical methods", *J. Vac. Sci. Technol. B* **13**(6), 2238–2244 (1995).
18. T. Yoshikawa, Y. Sugimoto, Y. Sakata, T. Takeuchi, M. Yamamoto, H. Hotta, S. Kohmoto, and K. Asakawa, "Smooth etching of various III/V and II/VI semiconductors by Cl₂ reactive ion beam etching", *J. Vac. Sci. Technol.* **B14**, 1764–1772 (1996).
19. S. Adashi, "GaAs, AlAs, and Al_xGa_{1-x}As material parameters for use in research and device applications", *J. Appl. Phys.* **58**, R1–R29 (1985).
20. P. Kupecek, J.M. Weulersse, P. Isnard, M. Alexandre, and M. Clerc, "Dispositif constitué d'un oscillateur paramétrique optique et d'un convertisseur de fréquence et optimisé pour la photochimie isotopique de UF₆ par laser", *J. Optics (Paris)* **14**, N°1, 43–48 (1983).